Desalination and Water Treatment
www.deswater.com

doi: 10.1080/19443994.2015.1066712

57 (2016) 14496–14505
July

Taylor & Francis
Taylor & Francis Group

Adsorption kinetics of p-nitrophenol (PNP) on coal-based activated carbon: experimental and simulation

Yan Shao[a,*], Huanhao Chen[b]

[a]*School of Chemical and Environmental Engineering, Wuyi University, Jiangmen 52920, P.R. China, Tel. +86 0750 3299397; email: wyuchemsy@126.com*
[b]*Department of Chemical Engineering, University of Puerto Rico-Mayagüez Campus, Mayagüez, PR 00681-9000, USA, email: huanhao.chen@upr.edu*

Received 21 October 2014; Accepted 20 June 2015

ABSTRACT

The adsorption kinetics of p-nitrophenol (PNP) on coal-based activated carbon (CBAC) inside a finite stirred batch adsorber has been investigated using different initial concentrations of PNP solution and different adsorbent dosages. The mathematical models including homogeneous surface diffusion model (HSDM) and pore surface diffusion model (PSDM) have also been applied to predict the adsorption kinetics of PNP on CBAC. The mathematical models were solved numerically by finite element method, and film mass transfer coefficient (k_f), surface diffusivity (D_s), and pore diffusivity (D_p) were obtained using nonlinear least square method. The results deduce that the effects of initial concentrations of PNP and adsorbent dosages on the values of k_f and D_s are very little. It has been also demonstrated that the intraparticle diffusion is the main controlling step through the adsorption process. Sensitivity analysis of HSDM and PSDM has been also studied using the error sum of squares (ESS) method. The results prove that all the models are sensitive to k_f and D_s, but the PSDM is insensitive to D_p.

Keywords: Adsorption; Surface diffusivity; Pore diffusivity; p-Nitrophenol; Concentration decay curve

1. Introduction

The removal of organic contaminants such as p-nitrophenol (PNP) and other phenolic derivatives from contaminated water has gained more and more attention [1,2]. There are many different methods such as chemical oxidation, solvent extraction, and carbon adsorption in order to decrease the amount of phenolic derivatives [3,4]. Among them, adsorption technology is a very useful method for removing organic contaminants from wastewater steams especially for treating low concentration of phenolic derivatives [5–7]. In recent years, many potential adsorbents have been developed for the treatment of wastewater [8,9]. However, granular activated carbons (GAC) as common adsorbents still have been extensively applied in the removal of organic contaminants in industrial due to their great advantages such as high surface areas, high micropores volume, and adsorption capacity [10].

It is well known that the equilibrium and kinetics parameters are significant factors for designing batch adsorption vessel and fixed-bed column adsorbers.

*Corresponding author.

Equilibrium data and parameters can be easily collected from experimental results. However, it is very difficult to obtain accurate kinetics data and parameters. Various mathematical models have been proposed to investigate adsorption kinetics. Among these mathematical models, pseudo-first-order model [2,11] and pseudo-second-order model [3,12–14] are two most commonly used kinetics models. However, both pseudo-first-order and pseudo-second-order models are unable to predict kinetic parameters and clearly describe the adsorption process [14]. Hence, conceptual models which can accurately describe the complex adsorption process have been also proposed. For instance, homogeneous surface diffusion model (HSDM) [5] and pore surface diffusion model (PSDM) [13,15] have been widely used to analyze the mechanism of intrapartical diffusion and obtain the kinetic parameters. Weber and Chakravorti [16] applied the HSDM and PSDM to investigate the adsorption kinetic parameters in fixed-bed adsorbers when the isotherm is linear and nonlinear.

The analysis solutions to the kinetic models such as HSDM and PSDM require that the external film resistance is negligible and the adsorbate concentration surrounding the particle is subjected to a step change and remains constant [17,18]. In fact, the film mass transfer resistance should be considered and the solution concentration decreased with the time during adsorption. So it is important to find a method which could accurately and simultaneously obtain kinetic parameters such as film mass transfer coefficient (k_f), surface diffusivity (D_s), and pore diffusivity (D_p). There are various methods to solve HSDM or PSDM such as diagrammatizing analytical technique [19] or by solving D_s after k_f obtained from empirical equation [20]. There are various empirical equations of k_f which involved the relationship of Sherwood number (*Sh*) and Reynolds number (*Re*) [21]. However, for most employed Wilson–Geankoplis equation to calculate k_f entails an estimation error of approximately 15% [22]. Though HSDM and PSDM have been widely used to investigate the adsorption process; however, very little literatures comparatively analyze the adsorption kinetic parameters through both the error sum of squares (ESS) and confidence interval (CI) analysis method based on these models.

The main objectives of the current work were to (1) study the adsorption kinetics of PNP on Coal-Based Activated Carbon (CBAC) inside a finite stirred batch adsorber; (2) analyze the adsorption kinetics using mathematical models including HSDM and PSDM; (3) sensitivity analysis of HSDM and PSDM through the ESS is investigated.

2. Experimental

2.1. Materials and analytical procedure

CBAC was purchased from Shanghai Xing Chang Activated Carbon Co., Ltd. (Shanghai, China). The activated carbons were washed with deionized water to remove fine carbon and leachable matter and dried at 105°C for 24 h. The particles are assumed to be spheres with a diameter of 2.4 mm according to the arithmetic mean. PNP was supplied by Guangzhou Chemical Reagent Factory (AR grade, Guangzhou, China). The concentration of the PNP solution was measured using UV spectrophotometry (VARIAN carry 50, American) at wavelengths of 317 nm.

2.2. Batch adsorption equilibrium

Adsorption isotherm experiments were measured using the "bottle point" procedure. In a typical experiment, 0.1 g carbon and 0.05 L PNP solution (concentrations from 200 to 2,500 mg/L) were added into a 0.1 L Erlenmeyer flask. The flasks were tightly sealed and shaken at 40 rpm in a temperature controlled incubator shaker at 25°C for 24 h. The amount of each solute adsorbed on the carbon at equilibrium was calculated from the mass balance of solute between carbon and solution as:

$$q_{eq} = \left(C_0 - C_{eq}\right)\frac{V_s}{W_s} \tag{1}$$

where $C_{\gamma 0}$ and C_{eq} are initial and equilibrium concentrations of adsorbate solution, respectively, mg/L. q_{eq} is a certain solute concentration in the adsorbent, mg/g.

2.3. Batch adsorption kinetics

Adsorption kinetic experiments were carried out in a stirred batch adsorber. A 1-L adsorber vessel was used to fill with a volume of 0.5 L of PNP solution. Agitator was provided by two bladed, flat impeller of 0.0065 m diameter. The impeller was driven by IKA RW20 digital electric motor (Specimen Model Factory, Shanghai, China) agitated the solution. The blades were set at the one-third of the bottom of vessel. The vessel was immersed in a constant temperature bath (25°C). The experiments were performed at five different initial known concentrations of PNP solution: 500, 1,000, 1,500, 2000, 2,500 mg/L, and at different activated carbon dosages: 3, 6, 9 g GAC/500 L PNP solution.

The agitation started immediately as the contact happened and the agitation speed was 300 rpm. The change in concentration was determined by measuring the UV spectrophotometry at specific time intervals. The volume of the solution was assumed to remain constant throughout the experiment.

3. Adsorption equilibrium and kinetic models

The adsorption mechanism of PNP on GACs can be described by three steps: (1) adsorbate molecules transport across the liquid film surrounding the solid particles; (2) adsorbate molecules adsorption at a specific surface site; (3) mass transport of adsorbate molecules in GAC particles. Step one or three are often the rate-limiting steps during the adsorption process [15]. The schematic representation of the particle can be seen in the Fig. 1.

3.1. Adsorption isotherm model

The adsorption equilibrium of PNP on GAC may be correlated with Freundlich equation:

$$q = KC^{1/n} \tag{2}$$

where q is adsorption capacity (mg/g), C in the concentration of PNP (mg/L), respectively.

3.2. Homogeneous surface diffusion model

The HSDM assumes that adsorbent is perfectly spherical with smooth diffusion surface. The intra-particle diffusion is governed by surface diffusion.

Mass balance in the adsorbent shell is given as:

$$\frac{\partial q}{\partial t} = \left(\frac{D_s}{r^2}\right)\frac{\partial}{\partial r}\left(r^2\frac{\partial q}{\partial r}\right) \tag{3}$$

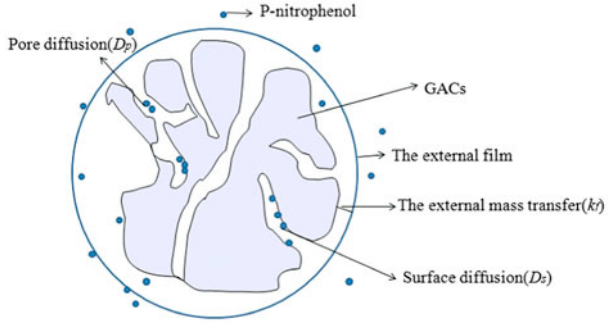

Fig. 1. The schematic representation of the particle adsorption.

External mass transfer is governed by a linear driving force in Eq. (4).

$$\rho_s\frac{\partial \bar{q}}{\partial t} = k_f a_p(C_t - C_s) \tag{4}$$

The average amount adsorbed into adsorbent at any time may be calculated with Eq. (5).

$$\bar{q} = \frac{3}{r_p^3}\int_0^{r_p} qr^2\,dr \tag{5}$$

The solute concentration in the solution calculated with mass balance as follows:

$$C_t = C_0 - \frac{\bar{q}\times W_s}{V_s} \tag{6}$$

The solution overcomes the mass transfer resistance of external film to reach the surface of the spherical adsorbent, and then is adsorbed in the adsorbent. The diffusion rate at the surface may be equal to the accumulation in the adsorbent as in Eq. (7).

$$\frac{\partial \bar{q}}{\partial t} = D_s a_p\left.\frac{\partial q}{\partial r}\right|_{r=r_p} \tag{7}$$

Equilibrium occurs between adsorbate concentration in the fluid and adsorbate load on the surface. Plus the symmetry of sphere, the initial condition, and boundary conditions constructed with Eqs. (8) and (9).

$$\text{I.C.}: q|_{t=0} = 0 \tag{8}$$

$$\text{B.C.}: \left.\frac{\partial q}{\partial r}\right|_{r=0} = 0;\ D_s a_p\left.\frac{\partial q}{\partial r}\right|_{r=r_p} = \frac{k_f}{\rho_s}a_p(C_t - C_s) \tag{9}$$

Dimensionless variables are introduced to minimize the variables of the number parameters and reduce the amount of rigorous numerical calculation.

$$R = \frac{r}{r_p},\ C_t^* = \frac{C_t}{C_0},\ C_s^* = \frac{C_s}{C_0},\ q^* = \frac{q}{q_0},\ \bar{q}^* = \frac{\bar{q}}{q_0} \tag{10}$$

The kinetic parameters are transformed to

$$D_s^* = \frac{D_s}{r_p^2},\ k_f^* = \frac{k_f}{r_p} \tag{11}$$

Then the model can be written as:

$$\frac{\partial q^*}{\partial t} = \frac{D_s^*}{R^2}\frac{\partial}{\partial R}\left(R^2\frac{\partial q_t^*}{\partial R}\right)_{R=1} \quad 0<R<1 \tag{12}$$

$$\text{I.C.} : q^*|_{t=0} = 0$$

$$\text{B.C.} : \left.\frac{\partial q^*}{\partial R}\right|_{R=0} = 0; \quad \frac{q_0}{C_0}D_s^* a_p \left.\frac{\partial q^*}{\partial R}\right|_{R=1} = \frac{k_f^*}{\rho_s}a_p(C_t^* - C_s^*)$$

3.3. Pore surface diffusion model

PSDM assumes that the adsorbent has a homogeneous pore distribution structures with effective pore diffusivity and surface diffusivity. When the adsorbates diffuse on the surface of pore wall by the hopping mechanism, it is "surface diffusion." When the adsorbates are transported by the diffusion in the pore fluid, it is "pore diffusion." The pore diffusion ensures the ease of mass transport inside the pores of the adsorbent. The two processes proceed in parallel, they are called "combined diffusion" [23].

Mass balance in the adsorbent shell is given as:

$$\rho_t(1-\varepsilon_p)\left(\frac{\partial q}{\partial t}\right) + \varepsilon_p\frac{\partial c_p}{\partial t} = \frac{1}{r^2}\frac{\partial}{\partial r}\left(r^2\varepsilon_p D_p\frac{\partial c_p}{\partial r} + r^2\rho_t(1-\varepsilon_p)D_s\frac{\partial q}{\partial r}\right) \tag{13}$$

where $\frac{\partial c_p}{\partial t} = \frac{\partial c_p}{\partial q}\frac{\partial q}{\partial t'}$, $\frac{\partial c_p}{\partial r} = \frac{\partial c_p}{\partial q}\frac{\partial q}{\partial r'}$, $\frac{\partial c_p}{\partial q} = \frac{n}{K}\left(\frac{q}{K}\right)^{n-1}$.

External mass transfer is governed by a linear driving force as in Eq. (14). And the average amount adsorbed into adsorbent and pore are calculated in Eqs. (5) and (15), respectively.

$$\frac{\partial \bar{q}}{\partial t} = k_f a_p(C_t - c_{ps}) \tag{14}$$

$$\bar{c}_p = \frac{3}{r_p^3}\int_0^{r_p} c_p r^2\, dr \tag{15}$$

c_{ps} is surface concentration equilibrium with bulk concentration at time t.

The solute concentration in the solution calculated with mass balance as follows:

$$C_t = \left(C_0 V_s - \bar{q}W_s - \frac{\bar{c}_p\varepsilon_p W_s}{\rho_s}\right)\frac{1}{V_s} \tag{16}$$

The diffusion rate at the pore and surface may be equal to the accumulation in the adsorbent as in Eq. (17).

$$\frac{\partial \bar{q}}{\partial t} = a_p\left[\varepsilon_p D_p\left.\frac{\partial c_p}{\partial r}\right|_{r=r_p} + (1-\varepsilon_p)D_s\rho_t\left.\frac{\partial q}{\partial r}\right|_{r=r_p}\right] \tag{17}$$

Intraparticle mass transfer is governed by pore diffusion and surface diffusion in parallel. Equilibrium occurs between adsorbed molecules and free molecules in the pore space within a particle. The initial condition and boundary conditions constructed with Eqs. (18) and (19).

$$\text{I.C.} : q|_{t=0} = 0 \tag{18}$$

$$\text{B.C.} : \left.\frac{\partial q}{\partial r}\right|_{r=0} = 0; \quad a_p\left[\varepsilon_p D_p\left.\frac{\partial c_p}{\partial r}\right|_{r=r_p} + (1-\varepsilon_p)D_s\rho_t\left.\frac{\partial q}{\partial r}\right|_{r=r_p}\right] = k_f a_p(C_t - c_{ps}) \tag{19}$$

Dimensionless variables are as follows:

$$R = \frac{r}{r_p}, \quad c_p^* = \frac{c_p}{C_0}, \quad c_{ps}^* = \frac{c_{ps}}{C_0}, \quad q^* = \frac{q}{q_0}, \quad \bar{q}^* = \frac{\bar{q}}{q_0} \tag{20}$$

The kinetic parameters are transformed to

$$D_s^* = \frac{D_s}{r_p^2}, \quad D_p^* = \frac{D_p}{r_p^2}, \quad k_f^* = \frac{k_f}{r_p} \tag{21}$$

Then the model can be written as:

$$(1-\varepsilon_p)\rho_t q_0\left(\frac{\partial q^*}{\partial t}\right) + \varepsilon_p C_0\frac{\partial c_p^*}{\partial t} = \left(\frac{1}{R^2}\right)\frac{\partial}{\partial R}\left(R^2\varepsilon_p D_p^* C_0\frac{\partial c_p^*}{\partial R} + R^2(1-\varepsilon_p)\rho_t D_s^* q_0\frac{\partial q^*}{\partial R}\right) \tag{22}$$

$$\text{I.C.} : q^*|_{t=0} = 0$$

$$\text{B.C.} : \left.\frac{\partial q^*}{\partial R}\right|_{R=0} = 0$$

$$a_p\left[\varepsilon_p D_p^* C_0\left.\frac{\partial c_p^*}{\partial R}\right|_{R=1} + (1-\varepsilon_p)D_s^*\rho_t q_0\left.\frac{\partial q^*}{\partial R}\right|_{R=1}\right] = k_f^* a_p C_0(C_t^* - c_{ps}^*)$$

The HSDM and PSDM equations under the condition of Freundlich equilibrium isotherm was setup and solved by finite element method. k_f, D_s, and D_p were obtained through nonlinear least square method until ESS is least. ESS may be calculated in Eq. (23).

$$\mathrm{ESS} = \sum_{1}^{n} (C^*_{\mathrm{exp}} - C^*_t)^2 \tag{23}$$

C^*_{exp} is the experimental dimensionless concentration.

The simplex algorithm [24] is a direct search method which does not require derivatives of ESS about the parameters. The trust region algorithm and Levenberg–Marquardt algorithm require the numerical derivatives. These algorithms are used by turn to ensure the solution is optimal.

k_f, D_s, and D_p are supposed to be constants in solving partial differential equations. The above estimation, i.e. least squares estimation is a kind of point estimates, in which a single value is calculated as an estimate of the parameter. A CI may be calculated along with the point estimate of the same parameter, to show the reliability of the estimate. To the parameter χ to be estimated and a given number α ($0 < \alpha < 1$), if statistics T_1 and T_2 are present and enable the probability.

$$P(T_1 \le \chi \le T_2) = 1 - \alpha \tag{24}$$

$[T_1, T_2]$ is CI of χ at the confidence level $(1 - \alpha)$, which means that, it is $(1 - \alpha)$ 100% confident that the true value of the parameter χ is in CI $[T_1, T_2]$. Larger CI indicates less precise estimate of the parameter. The calculation process of CI can be seen in our previous work [25].

The solution of the model, the least squares estimation and CI calculation are programmed with the software MATLAB, which simultaneously determine values of k_f, D_s, and D_p in the finite bath adsorption system.

4. Results and discussion

4.1. Physical properties of GAC

The physical properties of the GACs such as porosity (ε_p) and apparent particle density (ρ_s) are determined by Micromeritics AutoPore IV 9500 (Micromeritics instrument corporation, American) through applying various levels of pressure to a GACs immersed in mercury. And the true density of the particle (ρ_t) can be calculated by the values of ε_p and ρ_s. The other physical properties of the GACs are determined ASAP 2010 instrument (Micromeritics instrument corporation, American) equipped with a flame ionization detector (FID) and a HP-5 capillary column using N_2 as carried gas. The physical properties of activated carbon are listed in Table 1.

The adsorption equilibrium experiments for PNP solution on activated carbon were carried out at 25.0℃ and initial concentration range of 200–2,500 mg/L. The adsorption equilibrium data for PNP solution were analyzed by nonlinear curve fitting analysis according to Freundlich equation. The adsorption equilibrium results are shown in Fig. 2. The equilibrium parameters of the isotherm are obtained by least squares method. The Freundlich parameters values of K and n are found to be 58.778 and 5.233, respectively.

4.2. Adsorption kinetics

4.2.1. HSDM for determining D_s and k_f

The adsorption kinetic experiments for PNP solution on activated carbon at 25.0℃ were carried out in a stirred batch adsorber using different adsorbent dosages and initial concentrations of PNP. Fig. 3 shows that the experimental results of solution concentrations and calculated solution concentrations according to the HSDM decrease with increasing time under the experimental conditions of different initial PNP concentrations and carbon dosages. According to our previous work, the higher precision of the parameter estimates can be obtained by combining several decay curves after comparing the CI of parameters [25]. Hence, in the present study, the same k_f and D_s were calculated by combining different initial concentrations and GACs dosages. And all kinetic parameters (k_f, D_s) solved are given in Table 2.

As can be seen in Fig. 3, the agreement between the experimental concentration decay curves and the

Table 1
Properties of CBAC

Property	Value
Porosity ε_p	0.35
BET surface area (S_{BET}, m^2/g)	562
Total pore volume (V_T, cm^2/g)	0.44
Micropore volume (V_M, cm^2/g)	0.32
Average pore diameter (d_{pore}, nm)	1.93
Average particle diameter (m)	2.40×10^{-3}
Apparent particle density (ρ_s, kg/m^3)	852
True density of the particle (ρ_t, kg/m^3)	1,313

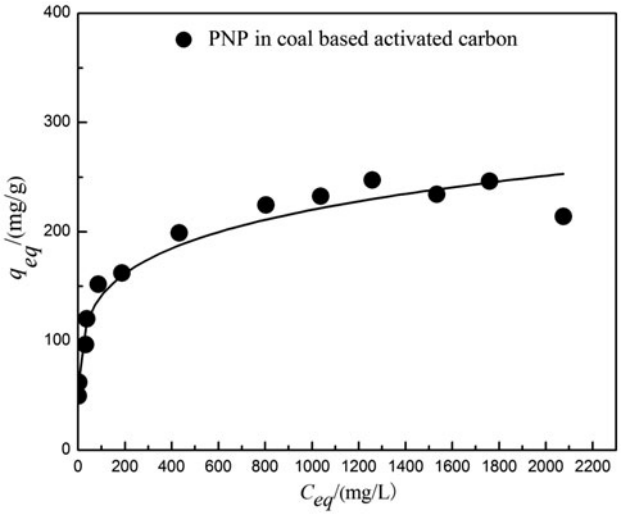

Fig. 2. Adsorption isotherm of PNP on CBAC at 25℃.

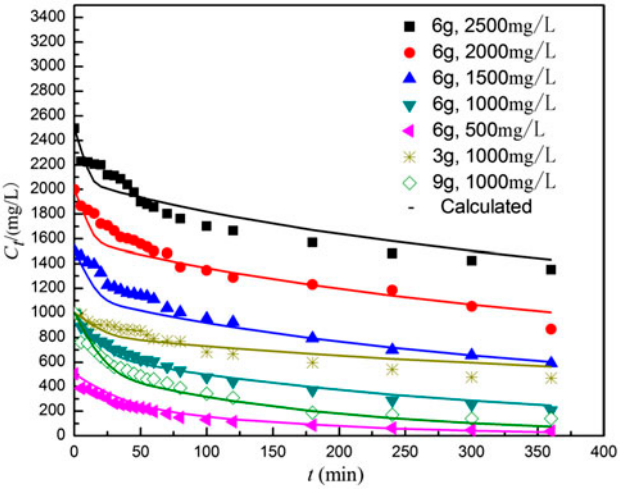

Fig. 3. Simulated results of CBAC using HSDM.

calculation theory concentration decay curves is quite good. Combined the results in Table 2, it can be observed that changing initial concentrations and adsorbent dosages have no effects on the kinetic values (k_f, D_s). The conclusion is in agreement with the literature reported by McKay [26], using the collocation solution method to get the same k_f and D_s in different initial solution concentrations and adsorbent dosages of three adsorption systems. However, at the initial period in Fig. 2, there is a slight deviation between experimental data and simulated data. The possible reason is that D_s is not a complete constant during the whole adsorption process, but may also dependent on the surface concentration of PNP. When adsorbate molecules loading less than a monolayer coverage in a given system, the surface diffusivity increases rapidly with the increase in loading [18]. When constant surface diffusivity was used, the actual surface diffusion rate is lower than simulated rate at the beginning segments of adsorption, hence, calculation theory concentrations decrease more rapidly than the experimental concentrations. However, based on the agreement between the experimental concentration decay curves and the calculation theory concentration decay curves, it is quite reasonable to regard D_s as a constant during this whole adsorption kinetic calculation process. And the kinetic values are considered to be constants with obvious significance for the design of fixed-bed adsorption in industry.

In Table 2, the value of k_f is much larger than D_s, indicating that the surface diffusion is the rate-controlling step. In the meantime, both of the two kinetic parameters are calculated. Therefore, the analytical solution to HSDM is reasonable but not accurate, especially when the process of adsorption is controlled not only by intraparticle diffusion.

4.2.2. PSDM for determining D_s, D_p and k_f

The values of k_f, D_s, and D_p were also calculated according to the PSDM. And the results are listed on Table 3. It can be clearly observed in Fig. 4 that the calculated results using the PSDM are in agreement with the experimental results. As can be seen in Fig. 4, the shape of theoretical concentration decay curves is similar to that in Fig. 3, which may also be explained by variable D_s.

Comparing with the kinetic values of HSDM and PSDM, the values of k_f and D_s are nearly same. The values of kinetic parameters decreased in the following order: $k_f > D_p > D_s$. It confirmed that the intraparticle diffusion mechanisms control the adsorption rate. The value of D_p is larger than D_s, indicating

Table 2
Surface diffusivity and external mass transport coefficient predicted by HSDM

$D_s \times 10^{12}$ (m^2/s)	CI $\times 10^{12}$ (m^2/s)	$k_f \times 10^6$ (m/s)	CI $\times 10^6$ (m/s)	ESS
1.038	[0.841, 1.072]	6.810	[6.808, 6.811]	0.4318

Table 3
Surface diffusivity, pore diffusivity, and external mass transport coefficient predicted by PSDM

$D_s \times 10^{12}$ (m^2/s)	CI $\times 10^{12}$ (m^2/s)	$D_p \times 10^8$ (m^2/s)	CI $\times 10^6$ (m^2/s)	$k_f \times 10^6$ (m/s)	CI $\times 10^6$ (m/s)	ESS
1.034	[0.829, 1.076]	1.334	[−1.512, 1.555]	6.754	[6.753, 6.754]	0.4332

that the surface diffusion is the controlling step in intraparticle diffusion. These results are in agreement with the previous results reported by London-van der Waals [27] and Hiroshi Komiyama and Smith [28].

4.2.3. Sensitivity analysis

It is very important to assess the influence of every kinetic parameters employed in HSDM and PSDM. Sensitivity analysis quantifies the magnitude of the effect of each variable affects on the simulated results using the least square method by increasing or decreasing the variables. Forty-one different k_f (from One five-hundredth of $k_{f\ Optimal}$ to three hundred times of $k_{f\ Optimal}$) as variables are chosen to calculate ESS when D_s and D_p are fixed. The treatment process of D_s and D_p is the same as k_f. When the values of D_s or D_p change, 41 different ESS can be also calculated. $k_{f\ Optimal}$ and $D_{s\ Optimal}$ used in sensitivity analysis of HSDM can be seen in Table 1; $k_{f\ Optimal}$, $D_{s\ Optimal}$, and $D_{p\ Optimal}$ used in sensitivity analysis of PSDM are obtained from Table 2.

The output variable (ESS) have a relationship of the model parameter vector x ($k_f/k_{f\ Optimal}$, $D_s/D_{s\ Optimal}$, $D_p/D_{p\ Optimal}$), which contained all parameters calculated in the previous section.

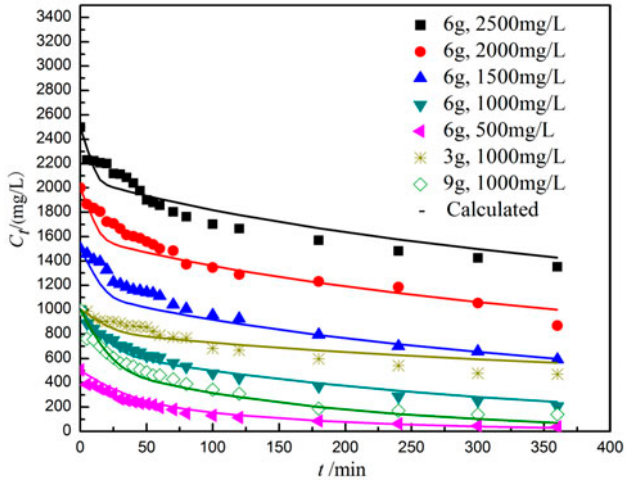

Fig. 4. Simulated results of CBAC using PSDM.

where

$$x = \frac{k_f}{k_{f\ optimal}} \quad \text{or} \quad x = \frac{D_s}{D_{s\ optimal}} \quad \text{or} \quad x = \frac{D_p}{D_{p\ optimal}} \tag{25}$$

In order to make data uniform and dimensionless, the x-Abscissa use semi-logarithmic coordinates. Figs. 5 and 6 show the sensitivity analysis results of HSDM and PSDM, respectively. As can be seen in Fig. 5, at left side of the lowest point ($x = 1$) where both k_f and D_s are decreasing, small changes in k_f have a more appreciable effect than D_s on residual sum of squares (ESS). That means when both mass transfer resistances and surface diffusion resistances increased, the model is more sensitive to k_f. D_s has a little influence on the model if intraparticle resistance is large enough in region (b). The right side of the lowest point is the opposite of the left side where HSDM is sensitive to D_s. And in the figure, there is a section (a) where both the k_f and D_s affect ESS. So in the section (a), The HSDM is sensitive to both film mass transfer coefficient and surface diffusivity in the particle. In the other part of the curves (region (a) or (c)), the adsorption is only controlled by film mass transfer or intraparticle diffusion.

As can be seen in Fig. 6, the shape of the curves of $k_f/k_{f\ Optimal}$ and $D_s/D_{s\ Optimal}$ is similar to Fig. 5. When the values of $D_p/D_{p\ Optimal}$ change, the values of ESS have no change comparing with the other curves. It indicates that the PSDM is more insensitive to the calculated value of D_p. The changing of D_p has slight effect on PSDM, meaning that the computed pore diffusivity is unreliable.

4.2.4. CI analysis

Correspondingly, the investigation of the CI of every parameter is also important for judging the parameters credibility. Because sensitive analysis only shows the effect of every parameter to the models, but not point out in which interval the calculated parameter is reliable., As can be seen in Tables 2 and 3, the CIs of k_f and D_s are much smaller than D_p when the CI is 95%, indicating that the calculated values of

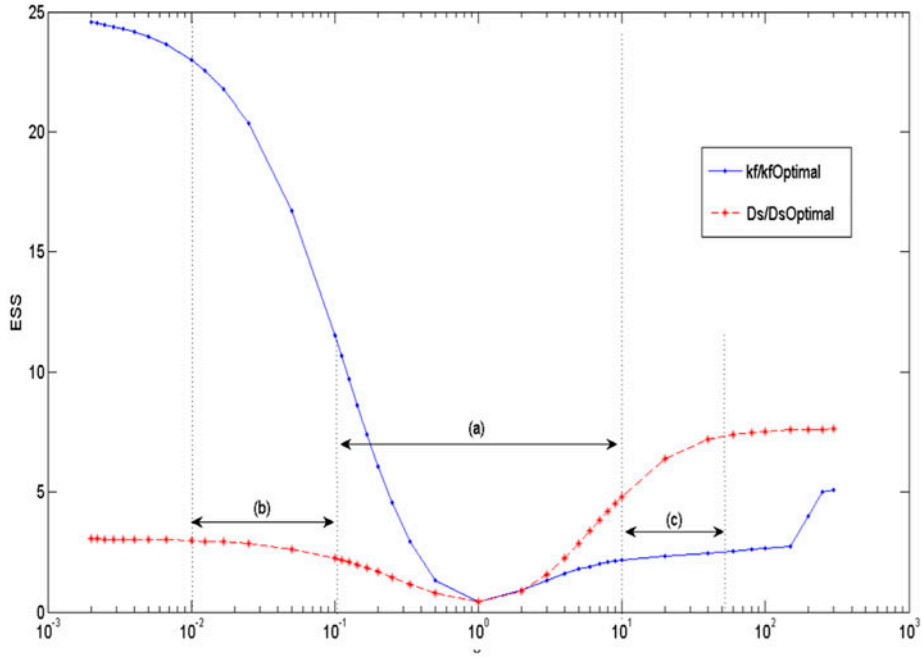

Fig. 5. Sensitivity evaluation of k_f and D_s in HSDM.

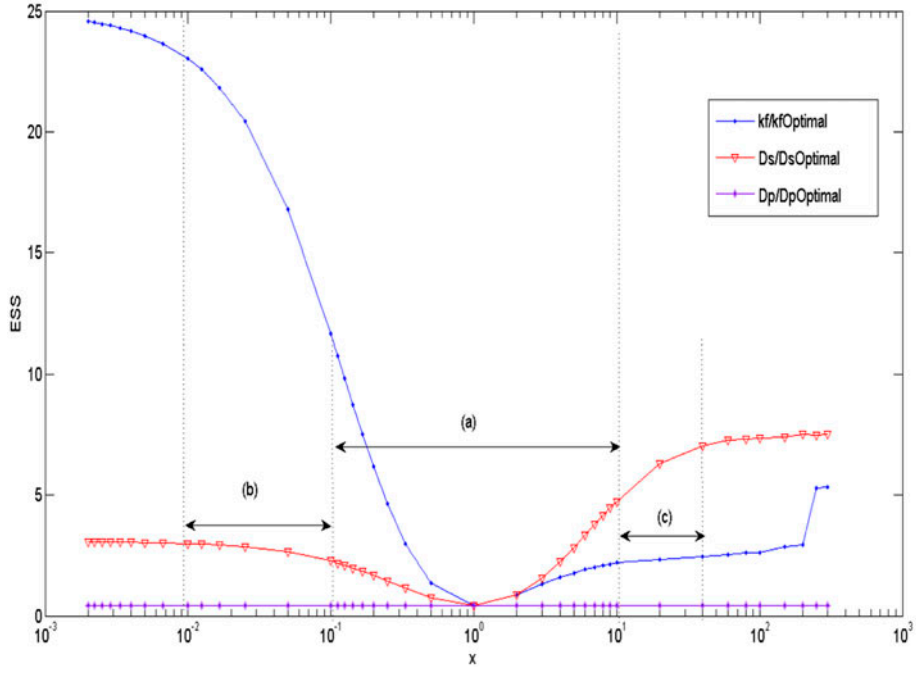

Fig. 6. Sensitivity evaluation of k_f, D_s and D_p in PSDM.

D_s and k_f have larger accuracy than D_p. The results in Tables 2 and 3 also confirm that the values of k_f and D_s are more reliable. The CI of k_f is smaller than D_s, confirming that the contribution of the film mass transfer resistance may be more significant than that of the surface diffusion. However, the surface diffusion cannot be neglected because that the corresponding CI is not large enough.

5. Conclusion

Liquid phase adsorption experiments of PNP on activated carbon were studied in a stirred batch adsorber. The experimental results were analyzed using the HSDM and PSDM. The implicit finite element scheme was also used for solving the HSDM and PSDM. The kinetic parameters of film mass transfer coefficient (k_f), surface diffusivities (D_s), and pore diffusivities (D_p) were evaluated by matching the experimental concentration decay data with a numerical solution of the mathematical model. The values of D_s and k_f calculated by HSDM are 1.038×10^{-12} m^2/s and 6.810×10^{-6} m/s, respectively. And the values of D_s, k_f and D_p calculated by PSDM are 1.034×10^{-12} m^2/s, 6.754×10^{-6} m/s and 1.334×10^{-8} m^2/s, respectively. All the calculated results indicate that intraparticle diffusion is controlled by the surface diffusion. However, the film mass transfer should not be neglected. Sensitivity analysis and CI analysis results also deduced that both HSDM and PSDM are sensitive to k_f, D_s and the PSDM is insensitive to D_p. It has proved that the values of k_f, D_s obtained from models are far more credible than the value of D_p.

Parameters of HSDM: C_0, C_t, C_s, q_0, q, $\bar{q}$, r_p, D_s, k_f, ρ_s; Parameters of PSDM : c_p, $\bar{c}_p$, c_{ps}, C_0, C_t, q_0, q, r_p, D_s, k_f, D_p, ε_p, ρ_t; Parameters of ESS method: C^*_{exp}, C^*_t.

Acknowledgment

Financial support by research fund of the Guangdong Natural Science Foundation (2014A030310164), Distinguished Yong Talents in Higher Education of Guangdong, China (2014KQNCX158), the fund of Jiangmen basic theory and scientific research projects (20140080091212), and the Science Foundation for Young Teachers of Wuyi University (NO. 2013zk11) are gratefully acknowledged. The authors are very grateful to Dr J. Guan for the helpful discussion about MATLAB programming.

Nomenclature

- a_p — surface area based on solid particle (m^2/m^3)
- C_t — fluid concentration at $t = t$ (C_0 at $t = 0$) (mg/L)
- C_s — fluid concentration in solution at $r = r_p$ (mg/L)
- C_p — fluid concentration in pore at $r = r$ and $t = t$ (mg/L)
- $\bar{C}p$ — fluid concentration in pore at $t = t$ (mg/L)
- C_{ps} — fluid concentration in pore at $r = r_p$ and $t = t$ (mg/L)
- D_s — surface diffusivity (m^2/s)
- D_p — pore diffusivity (m^2/s)
- k_f — fluid film mass transfer coefficient (m/s)
- q_0 — amount adsorbed in equilibrium with fluid concentration C_0 (mg/g)
- q — amount adsorbed at r and t (mg/g)
- $\bar{q}$ — average amount adsorbed in solid particle at $t = t$ (mg/g)
- q_s — average amount adsorbed in solid particle at $r = r_p$ and $t = t$ (mg/g)
- r_p — particle radius (m)
- t — time (s)
- ρ_s — apparent adsorbent density (kg/m^3)
- ρ_t — true density (kg/m^3)
- V_s — volume of vessel (m^3)
- W_s — mass of adsorbent (kg)
- ε_p — particle porosity

References

[1] A. Chakraborty, D. Deva, A. Sharma, N. Verma, Adsorbents based on carbon microfibers and carbon nanofibers for the removal of phenol and lead from water, J. Colloid Interface Sci. 359 (2011) 228–239.
[2] Y. Huang, H. Cao, Y. Lin, X. Wang, Z. cheng, Adsorption of phenol with the crosslinked polymer of P (MMA-MAh)-PEG 33, Desalin. Water Treat. 51 (2013) 6755–6760.
[3] Z. Ioannou, J. Simitzis, Adsorption kinetics of phenol and 3-nitrophenol from aqueous solutions on conventional and novel carbons, J. Hazard. Mater. 171 (2009) 954–964.
[4] B. Lai, Y.-H. Zhang, R. Li, Y.-X. Zhou, J. Wang, Influence of operating temperature on the reduction of high concentration p-nitrophenol (PNP) by zero valent iron (ZVI), Chem. Eng. J. 249 (2014) 143–152.
[5] D.O. Cooney, Adsorption design for wastewater treatment, CRC Press, Boca Raton FL, 1999.
[6] M. Ahmaruzzaman, D.K. Sharma, Adsorption of phenols from wastewater, J. Colloid Interface Sci. 287 (2005) 14–24.
[7] M.L. Soto, A. Moure, H. Domínguez, J.C. Parajó, Recovery, concentration and purification of phenolic compounds by adsorption: A review, J. Food Eng. 105 (2011) 1–27.
[8] M. Ahmaruzzaman, Industrial wastes as low-cost potential adsorbents for the treatment of wastewater laden with heavy metals, Adv. Colloid Interface Sci. 166 (2011) 36–59.
[9] M. Ahmaruzzaman, V.K. Gupta, Rice husk and its ash as low-cost adsorbents in water and wastewater treatment, Ind. Eng. Chem. Res. 50 (2011) 13589–13613.
[10] D.M. Nevskaia, E. Castillejos-Lopez, V. Muñoz, A. Guerrero-Ruiz, Adsorption of aromatic compounds from water by treated carbon materials, Environ. Sci. Technol. 38 (2004) 5786–5796.
[11] Z. Aksu, E. Kabasakal, Batch adsorption of 2,4-dichlorophenoxy-acetic acid (2,4-D) from aqueous solution by granular activated carbon, Sep. Purif. Technol. 35 (2004) 223–240.
[12] F. Zamora, E. Sabio, S. Román, C.M. González-García, Modelling the adsorption of p-Nitrophenol by the Boyd method in conjunction with the finite element method, Adsorpt. Sci. Technol. 28 (2010) 671–687.
[13] V. Ponnusami, K.S. Rajan, S.N. Srivastava, Application of film-pore diffusion model for methylene blue

adsorption onto plant leaf powders, Chem. Eng. J. 163 (2010) 236–242.
[14] E. Gonzo, L. Gonzo, Application of the film-pore diffusion model to the sorption of phenol onto activated carbons prepared from peanut shells, Adsorpt. Sci. Technol. 26 (2008) 651–659.
[15] D. Do, Adsorption analysis: Equilibria and kinetics, ICP, Singapore, 1998.
[16] T.W. Weber, R.K. Chakravorti, Pore and solid diffusion models for fixed-bed adsorbers, AlChE J. 20 (1974) 228–238.
[17] D.M. Ruthven, Principles of adsorption and adsorption processes, John Wiley & Sons, 1984.
[18] J. Crank, The mathematics of diffusion, Oxford University Press, 1979.
[19] J. Fujiki, N. Sonetaka, K.-P. Ko, E. Furuya, Experimental determination of intraparticle diffusivity and fluid film mass transfer coefficient using batch contactors, Chem. Eng. J. 160 (2010) 683–690.
[20] V.K.C. Lee, J.F. Porter, G. McKay, Fixed bed modelling for acid dye adsorption onto activated carbon, J. Chem. Technol. Biotechnol. 78 (2003) 1281–1289.
[21] G.Q. Wang, X.G. Yuan, K.T. Yu, Review of mass-transfer correlations for packed columns*, Ind. Eng. Chem. Res. 44 (2005) 8715–8729.
[22] K. Miyabe, Y. Kawaguchi, G. Guiochon, Kinetic study on external mass transfer in high performance liquid chromatography system, J. Chromatogr., A 1217 (2010) 3053–3062.
[23] H. Moon, W. Kook Lee, Intraparticle diffusion in liquid-phase adsorption of phenols with activated carbon in finite batch adsorber, J. Colloid Interface Sci. 96 (1983) 162–171.
[24] G. Seber, C. Wild, Nonlinear Regression, John Wiley & Sons, New York, NY, 1989.
[25] Y. Shao, H. Zhang, Y. Yan, Least squares estimation of kinetic parameters in batch adsorption of phenol with confidence interval analysis, Korean J. Chem. Eng. 30 (2013) 1544–1551.
[26] G. McKay, Solution to the homogeneous surface diffusion model for batch adsorption systems using orthogonal collocation, Chem. Eng. J. 81 (2001) 213–221.
[27] S. Baup, D. Wolbert, A. Laplanche, Importance of surface diffusivities in pesticide adsorption kinetics onto granular versus powdered activated carbon: Experimental determination and modeling, Environ. Technol. 23 (2002) 1107–1117.
[28] H. Komiyama, J. Smith, Surface diffusion in liquid-filled pores, AIChE J. 20 (1974) 1110–1117.